Robust generation of a magnonic cat state via a superconducting flux qubit

Yu-Bo Hou, Xin-Lei Hei, Xue-Feng Pan, Ji-Kun Xie, Ya-Long Ren, Sheng-Li Ma,* Fu-Li Li, and Peng-Bo Li†

MOE Key Laboratory for Non-Equilibrium Synthesis and Modulation of Condensed Matter, Shaanxi Province Key Laboratory of Quantum Information and Quantum Optoelectronic Devices, School of Physics, Xi'an Jiaotong University, Xi'an 710049, China

(Received 4 April 2024; accepted 8 July 2024; published 22 July 2024)

We study the hybrid system of a high-quality yttrium-iron-garnet (YIG) sphere magnetically coupled to a superconducting flux qubit via the magnetic fields created by two persistent-current quantum states. When the flux qubit is operated away from its sweet point, a coherent nonlinear two-magnon interaction can be predicted; that is, the qubit is excited by absorbing a pair of magnons. We show that the spontaneous emission of the qubit can be exploited to steer the magnon mode of the YIG sphere into a Schrödinger cat state with high fidelity. Our scheme has practical advantages in that it eliminates the need for precise control of the evolution time and the projective measurement, and is also insensitive to the qubit's pure dephasing.

DOI: 10.1103/PhysRevA.110.013711

I. INTRODUCTION

Quantum magnonics holds significant promise for developing various kinds of technological applications in quantum information science [1–8], owing to the exceptional properties exhibited by magnons, i.e., the bosonic collective spin excitations in magnetic materials. For the realization of coherent magnetic excitations and strong magnon coupling, the ferromagnetic material of yttrium iron garnet (YIG) has emerged as a preferred candidate. This preference depends on YIG's favorable properties, such as the low Curie temperature, exceptional magnetic quality, ultralow dissipation, and high spin density [9–26]. Experimentally, strong and ultrastrong couplings between the magnon mode in YIG and the microwave mode in the superconducting cavity have been reported [13,27–32], which make an ideal platform to provide opportunities for many quantum information applications [14,17,33–42]. Based on this composite quantum architecture, the indirect coupling between a magnon mode and a superconducting qubit can be mediated by adiabatically eliminating the cavity mode. Since the superconducting qubit has a strong anharmonicity, it can be used to generate nonclassical magnonic states [43–49] and detect single magnons [50–53].

On the other hand, recent advancements have demonstrated the feasibility of direct coupling between YIG magnets and superconducting qubits with naturally commensurate energies [54–60]. In comparison to indirect coupling via a microwave cavity, the direct one possesses some practical advantages. First, it enables a much larger coupling strength, such that the size of the magnetic materials can be effectively reduced. Moreover, the *in situ* tunability of this magnon-qubit system is beneficial for constructing large-scale magnonic quantum networks. In a recent work [54], Kounalakis *et al.* proposed an interesting approach for the generation of quantum superpositions of two distinguishable magnonic coherent states in a YIG particle directly coupled to a superconducting transmon qubit. It relies on a unitary dynamical evolution process, and the state-projection measurement is required at a specific point in time. Consequently, the fidelity of the target state may be easily affected by the decoherence of the qubit.

Different from Ref. [54], we put forward an efficient scheme for the robust generation of a magnonic cat state, where neither the unitary dynamics nor the projective measurement is required. The proposed scheme is based on a hybrid system of a high-quality YIG sphere magnetically coupled to a superconducting flux qubit via the magnetic fields created by two persistent-current quantum states. The key point is to induce both the transverse and longitudinal couplings, when the flux qubit is operated away from its degeneracy point. As a result, the interference of these two coupling terms leads to a strong two-magnon nonlinear interaction; that is, the magnon mode of the YIG sphere exchanges energy with the qubit in the form of magnon pairs. It is further shown that the spontaneous emission of the qubit as a resource can be utilized to drive magnetic excitations of the YIG sphere into a Schrödinger cat state. We emphasize here that since our scheme is based on a dissipative quantum state engineering process, it eliminates the need for precise control of the evolution time and the projective measurement, and is also immune to the pure dephasing of the qubit. The present result may have potential applications in the field of quantum computation and quantum sensing with hybrid magnonic systems.

II. MODEL

As illustrated in Fig. 1, we consider the hybrid architecture of a magnetic YIG sphere that is positioned at the center of a square superconducting flux qubit. The two persistent-current quantum states of the flux qubit generate the desired magnetic fields, which can give rise to a magnetic dipole coupling to the electron spins associated with the YIG sphere. In the

*Contact author: msl1987@xjtu.edu.cn
†Contact author: lipengbo@mail.xjtu.edu.cn

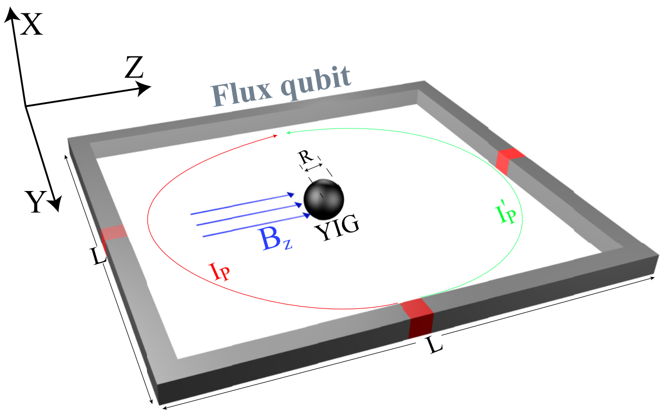

FIG. 1. The schematic diagram of the magnetically coupled hybrid architecture. It consists of a YIG sphere that is located at the center of a superconducting flux qubit with three Josephson junctions (the red markers on the loop). In addition, an external magnetic field B_z along the z direction is applied to the YIG sphere, which interacts with the flux qubit via the persistent currents I_P and I'_P, flowing in the clockwise and anticlockwise directions, respectively.

following, we will give a detailed description of the system's Hamiltonian.

A. Hamiltonian of the flux qubit

The flux qubit system is made up of three Josephson junctions as seen in Fig. 1, where one junction has a smaller Josephson energy than the two others. The distinct feature of this qubit is that it has two persistent-current quantum states, i.e., the clockwise one $|\curvearrowright\rangle$ and the anticlockwise one $|\curvearrowleft\rangle$. Due to the strong anharmonicity of the flux qubit, it can effectively serve as a two-level system, and the associated Hamiltonian under the basis $|\curvearrowright\rangle$ and $|\curvearrowleft\rangle$ is given by [61–63] (let $\hbar = 1$ hereafter)

$$H_{\mathrm{FQ}} = -\frac{\epsilon_z}{2}\sigma_z - \frac{\Delta_x}{2}\sigma_x. \tag{1}$$

Here, $\epsilon_z = 2I_P(\Phi_{\mathrm{ext}} - \frac{\Phi_0}{2})$ is the energy bias of the two current states, where I_P is the magnitude of the persistent current in the qubit and $\Phi_0 = \frac{h}{2e}$ is the magnetic flux quantum. The external magnetic flux Φ_{ext} penetrating the qubit loop yields the tunable parameter ϵ_z. Additionally, Δ_x is the tunnel splitting between the two current states, and σ_z and σ_x are the Pauli operators. Provided that we replace the junction with smaller Josephson energy with two identical Josephson junctions that form a dc superconducting quantum interference device (SQUID), the parameter Δ_x can also be controlled via the magnetic flux threading the SQUID loop [64,65].

B. Hamiltonian of the YIG

The isotropic Heisenberg Hamiltonian of the YIG sphere can be expressed as [1,2,66]

$$H_m = -2J\sum_{\langle i,j\rangle}\mathbf{S}_i\cdot\mathbf{S}_j + g_e\mu_B B_z\sum_i S_i^z. \tag{2}$$

The first term describes the ferromagnetic exchange interaction. Here, the sum with $\langle i, j\rangle$ denotes a summation over the nearestneighbor spins, where J is the coupling constant and $\mathbf{S}_i$ is the ith spin in the sphere. The second term describes the Zeeman effect influenced by the external magnetic field B_z along the z direction, where S_i^z is the spin projection operator, g_e is the electron g factor, and μ_B is the Bohr magneton.

By introducing the Holstein-Primakoff transformation [67], we can transform the spin operators into the new harmonic oscillators

$$S_i^+ = \sqrt{2S}\sqrt{1-\frac{a_i^\dagger a_i}{2S}}a_i, \quad S_i^- = \sqrt{2S}a_i^\dagger\sqrt{1-\frac{a_i^\dagger a_i}{2S}},$$
$$S_i^z = S - a_i^\dagger a_i. \tag{3}$$

In Eq. (3), $S_i^\pm = S_i^x \pm iS_i^y$ are the spin raising and lowering operators, and S is the spin quantum number, while $a_i^\dagger$ (a_i) is the mapped bosonic creation (annihilation) operator and obeys the standard commutation relation $[a_i, a_i^\dagger] = 1$. In the weak excitation limit, i.e., the total number of flipped spins in the system is much smaller than the total number of spins, the spin raising and lowering operators can be approximated as $S_i^+ \approx \sqrt{S}a_i$ and $S_i^- \approx \sqrt{S}a_i^\dagger$.

On the basis of the above transformations, we proceed to diagonalize the Hamiltonian H_m in Eq. (2) by using the plane-wave *Ansätze*

$$a_{\mathbf{k}} = \frac{1}{\sqrt{N}}\sum_{\mathbf{r}_i} e^{-i\mathbf{k}\cdot\mathbf{r}_i}a_i,$$
$$a_{\mathbf{k}}^\dagger = \frac{1}{\sqrt{N}}\sum_{\mathbf{r}_i} e^{i\mathbf{k}\cdot\mathbf{r}_i}a_i^\dagger, \tag{4}$$

where $\mathbf{r}_i$ is the position of the ith lattice site and N is the total number of spins in the YIG sphere. Under the long-wavelength limit, the H_m can be expressed as the summation of different magnon modes

$$H_m = \sum_{\mathbf{k}}\omega(\mathbf{k})a_{\mathbf{k}}^\dagger a_{\mathbf{k}}, \tag{5}$$

where $\omega(\mathbf{k}) \approx g_e\mu_B B_z + 4SJa_0^2|\mathbf{k}|^2$ is the dispersion relation, and a_0 is the lattice parameter. For our specific system, we only consider the Kittel mode $\mathbf{k} = 0$, which is a low-energy uniform mode regardless of the ferromagnetic exchange interaction [68]. For the Kittle mode, all spins precess with the same phase and amplitude, and all the precessing magnetizations are along the same direction in the YIG sphere. By neglecting the other modes $\mathbf{k} \neq 0$, the Hamiltonian of the YIG sphere can be simplified to

$$H_m = \omega a^\dagger a, \tag{6}$$

where $\omega = g_e\mu_B B_z$ is the eigenfrequency that can be well controlled via the biased magnetic field.

C. Interaction Hamiltonian between the flux qubit and the YIG sphere

Now let us consider the magnetic coupling between the flux qubit and the magnon mode in the YIG sphere. The magnetic field generated by the persistent current in the flux qubit is denoted as $\mathbf{B}_{\mathrm{FQ}}$, which has only a component along the x direction due to the given geometric configuration of

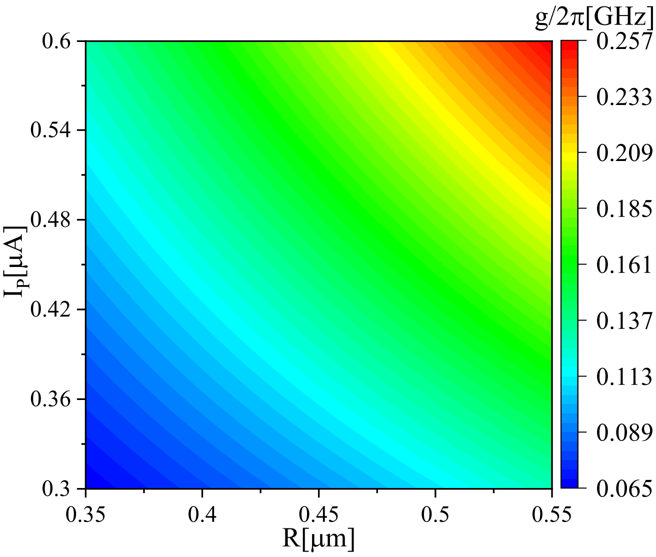

FIG. 2. The variation range of the magnon-qubit coupling strength g vs the the radius R and the persistent current I_P, where the side length L of the flux qubit is fixed at 10 μm.

the flux qubit (see Fig. 1). Therefore, two persistent-current quantum states $|\curvearrowright\rangle$ and $|\curvearrowleft\rangle$ produce different oppositely aligned magnetic fields $\sigma_z B^x_{\rm FQ}$, where $B^x_{\rm FQ}$ is the amplitude of the generated magnetic field at the center of the qubit loop. As a result, the magnetic interaction between the YIG sphere and the flux qubit takes the form $g_e\mu_B B^x_{\rm FQ}\sigma_z S^x$, where $S^x = \sum_i S^x_i$ is the collective spin operator. By using the bosonic operators a and $a^\dagger$, we can give the qubit-magnon interaction Hamiltonian

$$H_{\rm int} = g\sigma_z(a + a^\dagger), \tag{7}$$

where $g = \sqrt{N} g_e\mu_B B^x_{\rm FQ}\frac{\sqrt{2S}}{2}$ is the associated coupling strength.

To estimate the value of g, we choose the following parameters based on the current experiments. For a YIG sphere with the radius $R = 0.5$ μm and the spin density $\rho = 2.1 \times 10^{22}$ cm^{-3}, the contained total spin number is about $N \approx 1.1 \times 10^{10}$. For a flux qubit with the side length $L = 10$ μm and the persistent current $I_P = 0.4$ μA, the resulted magnetic field is $B^x_{\rm FQ} \approx 2\sqrt{2}\frac{\mu_0 I_P}{\pi L} \approx 4.5 \times 10^{-5}$ mT by means of the Biot-Savart law, where $\mu_0 = 4\pi \times 10^{-7}$ T m/A is the permeability of vacuum. Together with the physical constants $g_e = 2$ and $\mu_B = 9.274 \times 10^{-24}$ A m^2, we can calculate the magnetic magnon-qubit interaction $g \approx 2\pi \times 0.15$ GHz. Compared to the indirect coupling schemes by adiabatically eliminating the cavity mode [43–53], the direct one here can increase the magnon-qubit coupling strength by at least an order of magnitude. To gain a more comprehensive understanding, Fig. 2 shows the variation range of the coupling coefficient g in pace with the parameters R and I_P.

To sum up, we obtain the total Hamiltonian of the system:

$$H = \omega a^\dagger a - \frac{\epsilon_z}{2}\sigma_z - \frac{\Delta_x}{2}\sigma_x + g\sigma_z(a + a^\dagger). \tag{8}$$

Here $|\curvearrowright\rangle$ and $|\curvearrowleft\rangle$ are not the eigenstates of the flux qubit. To diagonalize the qubit's Hamiltonian, we bring in the dressed states

$$|g\rangle = \cos\frac{\theta}{2}|\curvearrowleft\rangle + \sin\frac{\theta}{2}|\curvearrowright\rangle, \quad E_g = -\frac{\nu}{2}, \tag{9}$$

$$|e\rangle = \sin\frac{\theta}{2}|\curvearrowleft\rangle - \cos\frac{\theta}{2}|\curvearrowright\rangle, \quad E_e = \frac{\nu}{2}, \tag{10}$$

where $|g\rangle$ and $|e\rangle$ denote the ground state and excited state of the flux qubit, respectively. In addition, the flux angle is defined as $\theta = \arctan(\frac{\Delta_x}{\epsilon_z})$, and the energy difference between the two dressed states is $\nu = \sqrt{\epsilon_z^2 + \Delta_x^2}$. Under the basis of these dressed states, Eq. (8) will be transformed to the form

$$H = \omega a^\dagger a + \frac{\nu}{2}\bar{\sigma}_z + g_z(a + a^\dagger)\bar{\sigma}_z + g_x(a + a^\dagger)(\bar{\sigma}^+ + \bar{\sigma}^-), \tag{11}$$

where we have $\bar{\sigma}_z = |e\rangle\langle e| - |g\rangle\langle g|$, $\bar{\sigma}^+ = |e\rangle\langle g|$, and $\bar{\sigma}^- = |g\rangle\langle e|$. Note that both the transverse coupling $g_x = g\sin\theta$ and the longitudinal coupling $g_z = g\cos\theta$ appear, which can give rise to a strong nonlinear two-magnon exchange interaction between the qubit and the magnon mode in the YIG sphere. This constitutes the key ingredients for the robust generation of a magnonic cat state.

III. GENERATION OF THE MAGNONIC CAT STATE

In this section, we will detail the procedure for the preparation of the magnonic Schrödinger cat state of the YIG sphere. The basic idea is to engineer a two-magnon driven-dissipative process, where the dissipation of the flux qubit as a resource is utilized to steer the magnon mode into a cat state.

A. Effective Hamiltonian

We start our discussion by deriving the effective Hamiltonian of the system. To this end, we first add an external microwave driving field resonantly applied to the flux qubit, which is described by the Hamiltonian $H_{\rm ext} = \Omega(\bar{\sigma}^+ e^{-i\omega_p t} + \bar{\sigma}^- e^{i\omega_p t})$, with the Rabi frequency Ω and the oscillating frequency ω_p. Combined with the Hamiltonian in Eq. (11), we then perform a unitary transformation $U = \exp[-i(a^\dagger a + \bar{\sigma}_z)\frac{\omega_p t}{2}]$ with $\omega_p = \nu$. The transformed Hamiltonian of the whole system yields

$$\begin{aligned} H' = {} & \Delta a^\dagger a + g_x(a\bar{\sigma}^- e^{-\frac{3}{2}i\nu t} + a\bar{\sigma}^+ e^{\frac{1}{2}i\nu t} \\ & + a^\dagger\bar{\sigma}^- e^{-\frac{1}{2}i\nu t} + a^\dagger\bar{\sigma}^+ e^{\frac{3}{2}i\nu t}) + g_z(a e^{-\frac{1}{2}i\nu t} + a^\dagger e^{\frac{1}{2}i\nu t})\bar{\sigma}_z \\ & + \Omega(\bar{\sigma}^+ + \bar{\sigma}^-), \end{aligned} \tag{12}$$

where the detuning is $\Delta = \omega - \frac{\nu}{2}$. To go a further step, we can draw support from the effective Hamiltonian to extract the time-averaged dynamics of this highly detuned quantum system, provided that the rapidly oscillating condition $\nu \gg \Delta, g_x, g_z, \Omega$ is satisfied in Eq. (12). As a result, the effective Hamiltonian of the system can be achieved (more details in the Appendix):

$$\begin{aligned} H_{\rm eff} = {} & \frac{8g_x^2}{3\nu}(|e\rangle\langle e| + 2a^\dagger a|e\rangle\langle e|) - g_{\rm eff}(a^2\bar{\sigma}^+ + a^{\dagger 2}\bar{\sigma}^-) \\ & + \Omega(\bar{\sigma}^+ + \bar{\sigma}^-), \end{aligned} \tag{13}$$

where $g_{\rm eff} = \frac{4g_x g_z}{\nu}$ and $\Delta = \frac{8g_x^2}{3\nu}$ have been used. It is now clear that the presence of transverse and longitudinal couplings can lead to an effective two-magnon exchange interaction, represented by the second term in Eq. (13). Unlike the usual Jaynes-Cummings model, here the qubit and the magnon mode in the YIG sphere exchange energy in the form of magnon pairs. It is a typical nonlinear qubit-magnon interaction; that is, the qubit is excited by absorbing a pair of magnons, and vice versa. By choosing the direct magnon-qubit coupling $g = 2\pi \times 0.15$ GHz, $g_x = g_z = \sqrt{2}g/2$ ($\theta = 45^\circ$), and $\nu = 2\pi \times 3$ GHz, we can work out the effective two-magnon coupling $g_{\rm eff} = 2\pi \times 15$ MHz. It provides opportunities for the efficient generation of the magnonic cat state via a two-magnon exchange process.

B. Quantum state engineering

Now we show how to prepare the magnonic cat state based on the Hamiltonian $H_{\rm eff}$. For this goal, we have to take into account the decoherence of the flux qubit, which acts as a quantum reservoir and loses magnons in pairs. Under the Markovian approximation, we can give the master equation that governs the time evolution of the density matrix ρ of the system:

$$\frac{d\rho}{dt} = -i[H_{\rm eff}, \rho] + \frac{\Gamma}{2}D[\bar{\sigma}^-]\rho + \frac{\Gamma_\phi}{4}D[\bar{\sigma}_z]\rho, \tag{14}$$

where Γ and Γ_ϕ represent the energy relaxation rate and the pure dephasing rate of the flux qubit [69], respectively, and $D[o]\rho = 2o\rho o^\dagger - \rho o^\dagger o - o^\dagger o\rho$ is the standard Lindblad operator. To clarify the mechanism of quantum state engineering, let us neglect the dissipation of the magnon mode, the effect of which will later be analyzed via numerical simulations.

The master Eq. (14) describes a two-magnon driven-dissipative process. To be specific, the flux qubit is resonantly driven by an external field, enabling the transition from the ground state $|g\rangle$ to the excited state $|e\rangle$. Then, the nonlinear term $g_{\rm eff}(a^2\bar{\sigma}^+ + a^{\dagger 2}\bar{\sigma}^-)$ will transfer a pair of magnons into the magnon mode. The above steps are equivalent to a two-magnon driven process. In contrast, the flux qubit can also absorb a pair of quanta from the magnon mode, and subsequently dissipate them into the environment via its spontaneous emission. This corresponds to a two-magnon dissipative process. Therefore, the competition of these two repumping and dissipation processes will force the whole system to eventually reach the steady state.

It is understandable that the steady state of the flux qubit is the ground state $|g\rangle$ due to its coupling to the bath, while the steady state of the magnon mode is the superposition of coherent states, the specific form of which is determined by its initial state [70]. This is because the magnon-number parity is conserved during the two-magnon quantum state engineering process, such that the final state depends on the parity of the initial state. If we initially prepare the magnon mode in the vacuum state (even parity), the final state of the system will take the form $|\Psi_s\rangle = |\Phi\rangle \otimes |g\rangle$, where $|\Phi\rangle$ is the even

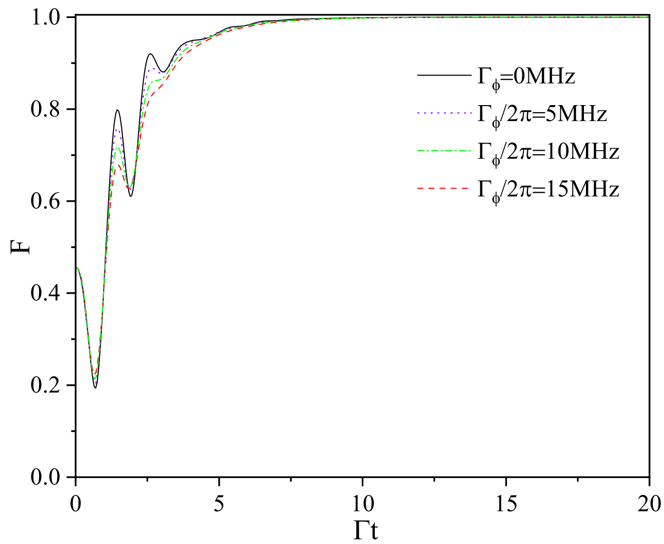

FIG. 3. Fidelity F vs the dimensionless variable Γt by numerically solving the master Eq. (14), where the initial state of the system is $|0\rangle \otimes |g\rangle$. The parameters are chosen as $g = \sqrt{2}g_x = \sqrt{2}g_z = 2\pi \times 0.15$ GHz, $\nu = 2\pi \times 3$GHz, $\Omega = 2\pi \times 33.75$ MHz, and $\Gamma = 2\pi \times 15$ MHz.

Schrödinger cat state

$$|\Phi\rangle = (|\alpha\rangle + |-\alpha\rangle)/\sqrt{2 + 2e^{-2\alpha^2}}, \tag{15}$$

with the displacement $\alpha = \sqrt{\frac{\Omega\nu}{4g_x g_z}}$. In addition, the amplitude α can be readily controlled by tuning the external driving microwave field. According to a dissipative quantum dynamical process, the magnonic cat state can be generated. As a consequence, it does not need the accurate control of the evolution time and the projective measurement, greatly loosening the requirement for the experimental implementation. To confirm the above discussion, we numerically solve master Eq. (14) with the system initialized in the state $|0\rangle \otimes |g\rangle$. Here we define the fidelity $F = {\rm Tr}[\rho_s\rho_m]$, where $\rho_s = |\Phi\rangle\langle\Phi|$ is the density matrix of the target state and $\rho_m = {\rm Tr}_{\rm qubit}(\rho)$ is the reduced density matrix of the magnon mode by tracing out the freedom of the qubit. Figure 3 displays the numerical result. With the time evolution, it is observed that the fidelity F converges to 1 at the steady state, implying that the magnon mode in the YIG sphere eventually evolves into the even cat state with $\alpha = 1.5$. Additionally, we can see that the presence of the qubit's pure dephasing has almost no effect on the quantum state preparation. This is due to the fact that the final state of the qubit is the ground state. In the subsequent discussion, we always set $\Gamma_\phi = 2\pi \times 15$ MHz.

To further elucidate the quantum characteristics of the generated state, we employ the Wigner function for validation, which has the form [71]

$$W(\alpha) = \frac{2}{\pi}\langle D(\alpha)PD(-\alpha)\rangle, \tag{16}$$

where $D(\alpha) = \exp(\alpha a^\dagger - \alpha^* a)$ is the state displaced operator, $P = \exp(i\pi a^\dagger a)$ is the parity operator, and $\langle\rangle$ denotes the expected value. It represents the quasiprobability distribution of a given quantum state in the phase space, enabling a

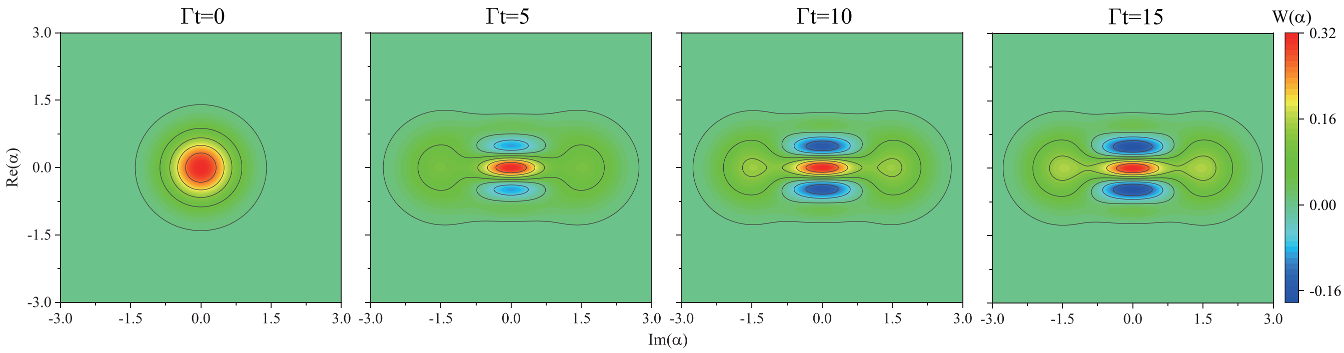

FIG. 4. Time evolution of the Wigner function by numerically solving the the master equation (14). Initial absence of negativity transitions to gradually pronounced negativity, culminating in an even cat state with $\alpha = 1.5$. The parameters are chosen the same as in Fig. 3.

visualization of its quantum features. Figure 4 illustrates the time evolution of the Wigner function from the initial magnonic vacuum state to an even cat state at the stationary state, i.e., $\Gamma t = 15$. In the phase space, two coherent states $|\pm\alpha\rangle$ with $\alpha = 1.5$ are observed to be localized in opposite sides. Meanwhile, the quantum interference of them leads to two negative peaks clearly, manifesting the nonclassical properties of the magnonic cat state.

Up to now, we have ignored the dissipation of the magnon mode in the YIG sphere, which is unavoidable and affects the fidelity of the desired state. In fact, its energy relaxation will break the conservation of parity during the quantum state preparation, thereby spoiling the coherence. However, for a large enough nonlinear coupling g_{eff}, the two-magnon process transiently dominates the dynamics, such that we can produce a high-fidelity magnonic state. In Fig. 5, we investigate the fidelity of the magnonic cat state by adding the dissipation term of the magnon mode into the master Eq. (14), where the energy damping rate is $\kappa = \alpha_G \omega$, and α_G is the Gilbert damping constant. In current experiments, α_G can typically reach the value of 10^{-5}–10^{-4} for a high-quality YIG sphere [2,50,54,72]. Even for the damping constant $\alpha_G = 1 \times 10^{-4}$, we can see that the fidelity $F > 0.97$ can still be achieved at the time points $\Gamma t = 10$ and 15. On the other hand, we also examine the impact of the magnon dissipation on the Wigner function. Figure 6 exhibits the time evolution of the Wigner function by considering the damping constant α_G. For the case of $\alpha_G = 1 \times 10^{-5}$, i.e., as seen in Fig. 6(a), the Wigner function in the whole phase space has negligible deviation from the ideal case $\alpha_G = 0$. Although there is a reduction of the Wigner negativity under the situation of $\alpha_G = 1 \times 10^{-4}$, i.e., as shown in Fig. 6(b), the quantum nature of the generated magnonic state is still clearly visible in the negative fringes of the Wigner function.

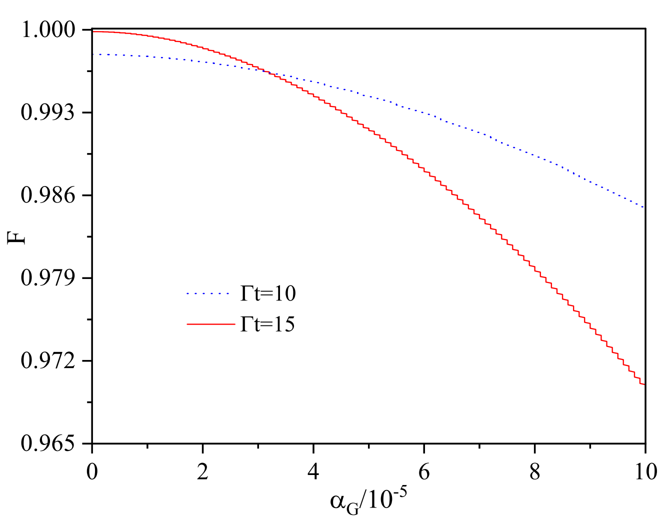

FIG. 5. Numerical result of the fidelity F vs the Gilbert damping constant α_G at the different evolution times $\Gamma t = 10$ and 15. The other parameters are chosen the same as in Fig. 3.

IV. CONCLUSION

Before concluding, we now discuss the experimental feasibility of our proposed scheme. For the flux qubit referring to experimentally achievable parameters [61,63,64], we select a persistent current of $I_P = 0.4$ μA and a side length of $L = 10$ μm, which can generate a magnetic field of $B^x_{\text{FQ}} = 4.5 \times 10^{-5}$ mT at the center of the qubit loop. Combined with the chosen radius of the YIG sphere $R = 0.5$ μm, our scheme can produce a direct coupling strength of $g \approx 2\pi \times 0.15$ GHz between the magnon mode and the qubit. Additionally, in our proposed model, the bias magnetic field of the YIG sphere is parallel to the qubit, ensuring that the bias field setting does not impact the qubit's performance. Based on these parameter settings and model design, our scheme can be experimentally implemented.

In conclusion, we have investigated the magnetic coupling between a high-quality YIG sphere and a superconducting flux qubit in detail, and proposed achieving a strong nonlinear two-magnon interaction by biasing the qubit away from its degeneracy point. Based on a well-designed two-magnon drive and dissipation process, we further showcase that the magnon mode in the YIG sphere can be driven into the Schrödinger cat state with high fidelity through the energy relaxation of the flux qubit. Our scheme has several distinct advantages. Unlike previous works that mostly rely on unitary dynamical evolution processes, our approach is based on a dissipative quantum state engineering process, and consequently neither the precise control of evolution time nor the projective measurement is required. Moreover, our scheme is insensitive to the pure dephasing of

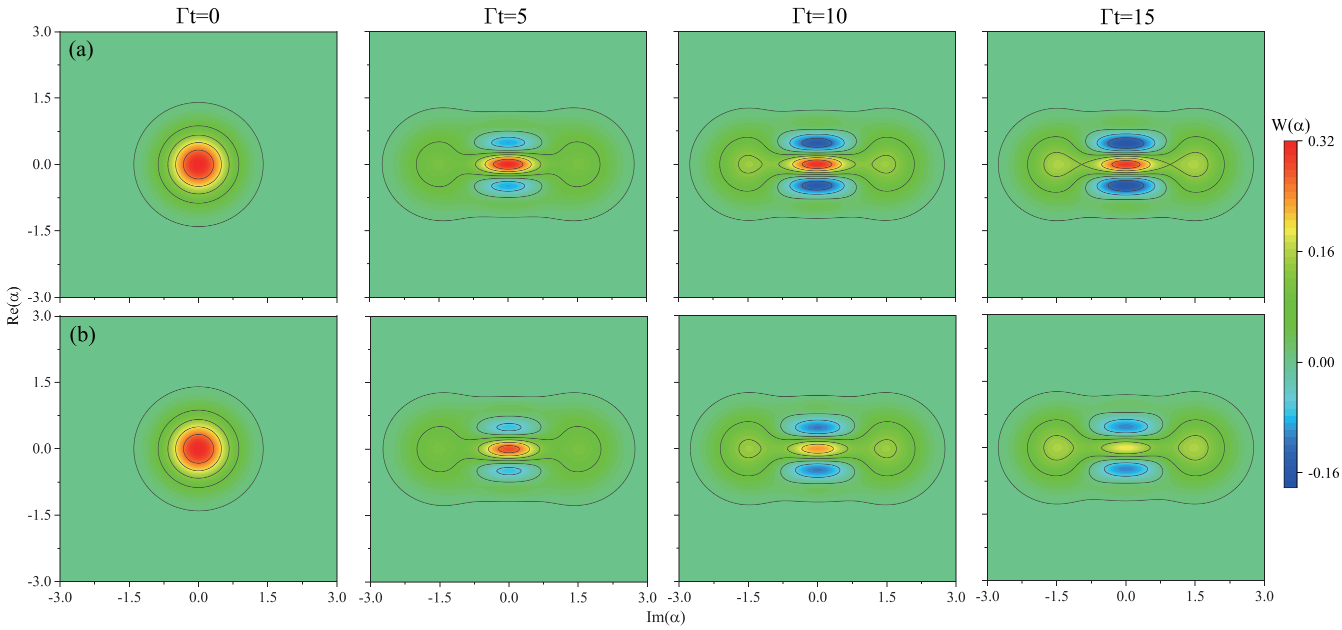

FIG. 6. Time evolution of the Wigner function in the presence of the energy damping of the magnon mode in the YIG sphere, i.e., the damping constant is $\alpha_G = 1 \times 10^{-5}$ for (a) and $\alpha_G = 1 \times 10^{-4}$ for (b). The other parameters are chosen the same as in Fig. 3.

the flux qubit, which makes it more feasible in realistic experiments.

ACKNOWLEDGMENTS

This work was supported by the National Natural Science Foundation of China (Grants No. 12375018, No. 11704306, and No. 12074307) and the Fundamental Research Funds for the Central Universities (Grant No. xzy022023002).

APPENDIX: DERIVATION OF THE EFFECTIVE HAMILTONIAN

Here, we provide a detailed derivation of the effective Hamiltonian Eq. (13) from the time-dependent Hamiltonian Eq. (12).

We denote the time-dependent part of Eq. (12) as $H_t'(t)$, which can be rewritten in the following form:

$$H_t'(t) = \sum_{m=1,2,3} h_m^\dagger e^{i\delta_m t} + \text{H.c.}, \tag{A1}$$

with $h_1^\dagger = g_x a\bar{\sigma}^+$, $h_2^\dagger = g_x a^\dagger \bar{\sigma}^+$, $h_3^\dagger = g_z a^\dagger \bar{\sigma}_z$, and $\delta_1 = \delta_3 = \frac{\nu}{2}$, $\delta_2 = \frac{3\nu}{2}$. Given that the condition $\nu \gg g_x, g_z$ is satisfied, the parameter δ_m in Eq. (A1) is sufficiently large. As a result, the system's large detuning condition is satisfied. Thus, we can substitute Eq. (A1) into the standard form of the effective Hamiltonian to obtain the effective Hamiltonian of $H_t'(t)$, denoted as H_{eff}^t, which takes the form [73]

$$H_{\text{eff}}^t = \sum_{m,n=1,2,3} -\frac{1}{\delta_n}[h_m^\dagger h_n^\dagger e^{i(\delta_m+\delta_n)t} + h_m h_n^\dagger e^{-i(\delta_m-\delta_n)t} - h_m^\dagger h_n e^{i(\delta_m-\delta_n)t} - h_m h_n e^{-i(\delta_m+\delta_n)t}]. \tag{A2}$$

Then, by employing the rotating-wave approximation and neglecting the rapidly oscillating terms, Eq. (A2) can be simplified to

$$H_{\text{eff}}^t = \sum_{n=1,2,3} \frac{1}{\delta_n}[h_n^\dagger, h_n] + \sum_{m,n=1,2,3}^{m<n} \frac{1}{\bar{\delta}_{mn}}\{[h_m^\dagger, h_n]e^{i(\delta_m-\delta_n)t} + \text{H.c.}, \tag{A3}$$

with $\bar{\delta}_{mn} = \frac{\delta_m+\delta_n}{2}$. By substituting the specific commutation relations of the operators, according to Eq. (A1), into Eq. (A3), we obtain

$$H_{\text{eff}}^t = \frac{8g_x^2}{3\nu}(2a^\dagger a|e\rangle\langle e| + |e\rangle\langle e| - a^\dagger a) + \frac{g_x^2}{\nu}(a^2\bar{\sigma}_z e^{-i\nu t} + a^{\dagger 2}\bar{\sigma}_z e^{i\nu t}) - \frac{g_x g_z}{\nu}(1 + 2a^\dagger a)(\bar{\sigma}^+ e^{i\nu t} + \bar{\sigma}^- e^{-i\nu t}) - \frac{4g_x g_z}{\nu}(a^{\dagger 2}\bar{\sigma}^- + a^2\bar{\sigma}^+), \tag{A4}$$

where $aa^\dagger = 1 + a^\dagger a$ and $|g\rangle\langle g| = 1 - |e\rangle\langle e|$ have been used. Now, by neglecting the rapidly oscillating terms in Eq. (A4) and including the time-independent terms from Eq. (12), the effective Hamiltonian of the system is

$$H_{\text{eff}} = \left(\Delta - \frac{8g_x^2}{3\nu}\right)a^\dagger a + \frac{8g_x^2}{3\nu}(2a^\dagger a|e\rangle\langle e| + |e\rangle\langle e|) - \frac{4g_x g_z}{\nu}(a^{\dagger 2}\bar{\sigma}^- + a^2\bar{\sigma}^+) + \Omega(\bar{\sigma}^+ + \bar{\sigma}^-). \tag{A5}$$

By setting $\Delta = \frac{8g_x^2}{3\nu}$, we can obtain the form of Eq. (13):

$$H_{\text{eff}} = \frac{8g_x^2}{3\nu}(|e\rangle\langle e| + 2a^\dagger a|e\rangle\langle e|) - g_{\text{eff}}(a^2\bar{\sigma}^+ + a^{\dagger 2}\bar{\sigma}^-) + \Omega(\bar{\sigma}^+ + \bar{\sigma}^-), \tag{A6}$$

with the effective two-magnon coupling $g_{\text{eff}} = \frac{4g_x g_z}{\nu}$.

[1] H. Y. Yuan, Y. Cao, A. Kamra, R. A. Duine, and P. Yan, Quantum magnonics: When magnon spintronics meets quantum information science, Phys. Rep. **965**, 1 (2022).

[2] B. Zare Rameshti, S. Viola Kusminskiy, J. A. Haigh, K. Usami, D. Lachance-Quirion, Y. Nakamura, C.-M. Hu, H. X. Tang, G. E. Bauer, and Y. M. Blanter, Cavity magnonics, Phys. Rep. **979**, 1 (2022).

[3] D. Lachance-Quirion, Y. Tabuchi, A. Gloppe, K. Usami, and Y. Nakamura, Hybrid quantum systems based on magnonics, Appl. Phys. Express **12**, 070101 (2019).

[4] Y. Tabuchi, S. Ishino, T. Ishikawa, R. Yamazaki, K. Usami, and Y. Nakamura, Hybridizing ferromagnetic magnons and microwave photons in the quantum limit, Phys. Rev. Lett. **113**, 083603 (2014).

[5] Y.-P. Wang, J. W. Rao, Y. Yang, P.-C. Xu, Y. S. Gui, B. M. Yao, J. Q. You, and C.-M. Hu, Nonreciprocity and unidirectional invisibility in cavity magnonics, Phys. Rev. Lett. **123**, 127202 (2019).

[6] S. P. Wolski, D. Lachance-Quirion, Y. Tabuchi, S. Kono, A. Noguchi, K. Usami, and Y. Nakamura, Dissipation-based quantum sensing of magnons with a superconducting qubit, Phys. Rev. Lett. **125**, 117701 (2020).

[7] Y. Yang, Y.-P. Wang, J. W. Rao, Y. S. Gui, B. M. Yao, W. Lu, and C.-M. Hu, Unconventional singularity in anti-parity-time symmetric cavity magnonics, Phys. Rev. Lett. **125**, 147202 (2020).

[8] P. Pirro, V. I. Vasyuchka, A. A. Serga, and B. Hillebrands, Advances in coherent magnonics, Nat. Rev. Mater. **6**, 1114 (2021).

[9] X. Zhang, C.-L. Zou, L. Jiang, and H. X. Tang, Cavity magnomechanics, Sci. Adv. **2**, e1501286 (2016).

[10] X. Zhang, C.-L. Zou, N. Zhu, F. Marquardt, L. Jiang, and H. X. Tang, Magnon dark modes and gradient memory, Nat. Commun. **6**, 8914 (2015).

[11] D. Zhang, X.-M. Wang, T.-F. Li, X.-Q. Luo, W. Wu, F. Nori, and J. You, Cavity quantum electrodynamics with ferromagnetic magnons in a small yttrium-iron-garnet sphere, npj Quantum Inf. **1**, 15014 (2015).

[12] A. A. Serga, A. V. Chumak, and B. Hillebrands, YIG magnonics, J. Phys. D **43**, 264002 (2010).

[13] L. Bai, M. Harder, Y. P. Chen, X. Fan, J. Q. Xiao, and C.-M. Hu, Spin pumping in electrodynamically coupled magnon-photon systems, Phys. Rev. Lett. **114**, 227201 (2015).

[14] A. Gardin, J. Bourhill, V. Vlaminck, C. Person, C. Fumeaux, V. Castel, and G. C. Tettamanzi, Manifestation of the coupling phase in microwave cavity magnonics, Phys. Rev. Appl. **19**, 054069 (2023).

[15] J. A. Haigh, A. Nunnenkamp, A. J. Ramsay, and A. J. Ferguson, Triple-resonant Brillouin light scattering in magneto-optical cavities, Phys. Rev. Lett. **117**, 133602 (2016).

[16] H. Y. Yuan, P. Yan, S. Zheng, Q. Y. He, K. Xia, and M.-H. Yung, Steady Bell state generation via magnon-photon coupling, Phys. Rev. Lett. **124**, 053602 (2020).

[17] G.-Q. Zhang, Y. Wang, and W. Xiong, Detection sensitivity enhancement of magnon Kerr nonlinearity in cavity magnonics induced by coherent perfect absorption, Phys. Rev. B **107**, 064417 (2023).

[18] X. Zhang, N. Zhu, C.-L. Zou, and H. X. Tang, Optomagnonic whispering gallery microresonators, Phys. Rev. Lett. **117**, 123605 (2016).

[19] M. Harder, B. M. Yao, Y. S. Gui, and C.-M. Hu, Coherent and dissipative cavity magnonics, J. Appl. Phys. **129**, 201101 (2021).

[20] F.-X. Sun, S.-S. Zheng, Y. Xiao, Q. Gong, Q. He, and K. Xia, Remote generation of magnon Schrödinger cat state via magnon-photon entanglement, Phys. Rev. Lett. **127**, 087203 (2021).

[21] H. Huebl, C. W. Zollitsch, J. Lotze, F. Hocke, M. Greifenstein, A. Marx, R. Gross, and S. T. B. Goennenwein, High cooperativity in coupled microwave resonator ferrimagnetic insulator hybrids, Phys. Rev. Lett. **111**, 127003 (2013).

[22] A. Navabi, Y. Liu, P. Upadhyaya, K. Murata, F. Ebrahimi, G. Yu, B. Ma, Y. Rao, M. Yazdani, M. Montazeri, L. Pan, I. N. Krivorotov, I. Barsukov, Q. Yang, P. Khalili Amiri, Y. Tserkovnyak, and K. L. Wang, Control of spin-wave damping in YIG using spin currents from topological insulators, Phys. Rev. Appl. **11**, 034046 (2019).

[23] Y. Li, W. Zhang, V. Tyberkevych, W.-K. Kwok, A. Hoffmann, and V. Novosad, Hybrid magnonics: Physics, circuits, and applications for coherent information processing, J. Appl. Phys. **128**, 130902 (2020).

[24] J.-X. Peng, A. Kundu, Z.-X. Liu, A. u. Rahman, N. Akhtar, and M. Asjad, Vector photon-magnon-phonon coherence in a polarized microwave driven cavity magnomechanical system, Phys. Rev. B **109**, 064412 (2024).

[25] X.-L. Hei, P.-B. Li, X.-F. Pan, and F. Nori, Enhanced tripartite interactions in spin-magnon-mechanical hybrid systems, Phys. Rev. Lett. **130**, 073602 (2023).

[26] X.-L. Hei, X.-L. Dong, J.-Q. Chen, C.-P. Shen, Y.-F. Qiao, and P.-B. Li, Enhancing spin-photon coupling with a micromagnet, Phys. Rev. A **103**, 043706 (2021).

[27] A. Osada, R. Hisatomi, A. Noguchi, Y. Tabuchi, R. Yamazaki, K. Usami, M. Sadgrove, R. Yalla, M. Nomura, and Y. Nakamura, Cavity optomagnonics with spin-orbit coupled photons, Phys. Rev. Lett. **116**, 223601 (2016).

[28] X. Zhang, C.-L. Zou, L. Jiang, and H. X. Tang, Strongly coupled magnons and cavity microwave photons, Phys. Rev. Lett. **113**, 156401 (2014).

[29] M. Goryachev, W. G. Farr, D. L. Creedon, Y. Fan, M. Kostylev, and M. E. Tobar, High-cooperativity cavity QED with magnons at microwave frequencies, Phys. Rev. Appl. **2**, 054002 (2014).

[30] Y. Li, T. Polakovic, Y.-L. Wang, J. Xu, S. Lendinez, Z. Zhang, J. Ding, T. Khaire, H. Saglam, R. Divan, J. Pearson, W.-K. Kwok, Z. Xiao, V. Novosad, A. Hoffmann, and W. Zhang, Strong coupling between magnons and microwave photons in on-chip ferromagnet-superconductor thin-film devices, Phys. Rev. Lett. **123**, 107701 (2019).

[31] J. T. Hou and L. Liu, Strong coupling between microwave photons and nanomagnet magnons, Phys. Rev. Lett. **123**, 107702 (2019).

[32] J. Bourhill, N. Kostylev, M. Goryachev, D. L. Creedon, and M. E. Tobar, Ultrahigh cooperativity interactions between magnons and resonant photons in a YIG sphere, Phys. Rev. B **93**, 144420 (2016).

[33] Z.-X. Liu, H. Xiong, M.-Y. Wu, and Y.-Q. Li, Absorption of magnons in dispersively coupled hybrid quantum systems, Phys. Rev. A **103**, 063702 (2021).

[34] Z.-H. Yuan, Y.-J. Chen, J.-X. Han, J.-L. Wu, W.-Q. Li, Y. Xia, Y.-Y. Jiang, and J. Song, Periodic photon-magnon blockade in

an optomagnonic system with chiral exceptional points, Phys. Rev. B **108**, 134409 (2023).

[35] S. Das, S. Chakraborty, and T. N. Dey, Gain-assisted controllable fast-light generation in cavity magnomechanics, Phys. Rev. A **108**, 033517 (2023).

[36] J.-K. Xie, S.-L. Ma, Y.-L. Ren, S.-Y. Gao, and F.-L. Li, Chiral cavity-magnonic system for the unidirectional emission of a tunable squeezed microwave field, Phys. Rev. A **108**, 033701 (2023).

[37] C. Zhao, Z. Yang, D. Wang, Y. Yan, C. Li, Z. Wang, and L. Zhou, Quantum networks assisted by dark modes in optomagnonic systems, Phys. Rev. A **108**, 043703 (2023).

[38] Y. Li, V. G. Yefremenko, M. Lisovenko, C. Trevillian, T. Polakovic, T. W. Cecil, P. S. Barry, J. Pearson, R. Divan, V. Tyberkevych, C. L. Chang, U. Welp, W.-K. Kwok, and V. Novosad, Coherent coupling of two remote magnonic resonators mediated by superconducting circuits, Phys. Rev. Lett. **128**, 047701 (2022).

[39] J. Li, Y.-P. Wang, J.-Q. You, and S.-Y. Zhu, Squeezing microwaves by magnetostriction, Natl. Sci. Rev. **10**, nwac247 (2022).

[40] R.-C. Shen, J. Li, Z.-Y. Fan, Y.-P. Wang, and J. Q. You, Mechanical bistability in Kerr-modified cavity magnomechanics, Phys. Rev. Lett. **129**, 123601 (2022).

[41] C. Zhao, Z. Yang, R. Peng, J. Yang, C. Li, and L. Zhou, Dissipative-coupling-induced transparency and high-order sidebands with Kerr nonlinearity in a cavity-magnonics system, Phys. Rev. Appl. **18**, 044074 (2022).

[42] R. Hou, W. Zhang, X. Han, H.-F. Wang, and S. Zhang, Magnon blockade based on the Kerr nonlinearity in cavity electromagnonics, Phys. Rev. A **109**, 033721 (2024).

[43] S. He, X. Xin, F.-Y. Zhang, and C. Li, Generation of a Schrödinger cat state in a hybrid ferromagnet-superconductor system, Phys. Rev. A **107**, 023709 (2023).

[44] Q. Guo, J. Cheng, H. Tan, and J. Li, Magnon squeezing by two-tone driving of a qubit in cavity-magnon-qubit systems, Phys. Rev. A **108**, 063703 (2023).

[45] J.-K. Xie, S.-L. Ma, and F.-L. Li, Quantum-interference-enhanced magnon blockade in an yttrium-iron-garnet sphere coupled to superconducting circuits, Phys. Rev. A **101**, 042331 (2020).

[46] X. Li, X. Wang, Z. Wu, W.-X. Yang, and A. Chen, Tunable magnon antibunching in a hybrid ferromagnet-superconductor system with two qubits, Phys. Rev. B **104**, 224434 (2021).

[47] F. Wang, C. Gou, J. Xu, and C. Gong, Hybrid magnon-atom entanglement and magnon blockade via quantum interference, Phys. Rev. A **106**, 013705 (2022).

[48] Y.-L. Ren, J.-K. Xie, X.-K. Li, S.-L. Ma, and F.-L. Li, Long-range generation of a magnon-magnon entangled state, Phys. Rev. B **105**, 094422 (2022).

[49] V. Azimi-Mousolou, A. Bergman, A. Delin, O. Eriksson, M. Pereiro, D. Thonig, and E. Sjöqvist, Transmon probe for quantum characteristics of magnons in antiferromagnets, Phys. Rev. B **108**, 094430 (2023).

[50] Y. Tabuchi, S. Ishino, A. Noguchi, T. Ishikawa, R. Yamazaki, K. Usami, and Y. Nakamura, Coherent coupling between a ferromagnetic magnon and a superconducting qubit, Science **349**, 405 (2015).

[51] D. Xu, X.-K. Gu, H.-K. Li, Y.-C. Weng, Y.-P. Wang, J. Li, H. Wang, S.-Y. Zhu, and J. Q. You, Quantum control of a single magnon in a macroscopic spin system, Phys. Rev. Lett. **130**, 193603 (2023).

[52] T. Ikeda, A. Ito, K. Miuchi, J. Soda, H. Kurashige, and Y. Shikano, Axion search with quantum nondemolition detection of magnons, Phys. Rev. D **105**, 102004 (2022).

[53] D. Lachance-Quirion, S. P. Wolski, Y. Tabuchi, S. Kono, K. Usami, and Y. Nakamura, Entanglement-based single-shot detection of a single magnon with a superconducting qubit, Science **367**, 425 (2020).

[54] M. Kounalakis, G. E. W. Bauer, and Y. M. Blanter, Analog quantum control of magnonic cat states on a chip by a superconducting qubit, Phys. Rev. Lett. **129**, 037205 (2022).

[55] H. Y. Yuan, J. Xie, and R. A. Duine, Magnon bundle in a strongly dissipative magnet, Phys. Rev. Appl. **19**, 064070 (2023).

[56] S. Yuan, C. Liu, J. Chen, S. Liu, J. Lan, H. Yu, J. Wu, F. Yan, M.-H. Yung, J. Xiao, L. Jiang, and D. Yu, Spin-wave-based tunable coupler between superconducting flux qubits, Phys. Rev. A **107**, 012434 (2023).

[57] Z.-Y. Jin and J. Jing, Magnon blockade in magnon-qubit systems, Phys. Rev. A **108**, 053702 (2023).

[58] M. Kounalakis, S. Viola Kusminskiy, and Y. M. Blanter, Engineering entangled coherent states of magnons and phonons via a transmon qubit, Phys. Rev. B **108**, 224416 (2023).

[59] Y. Fan, J. Li, and Y. Wu, Nonclassical magnon pair generation and Cauchy-Schwarz inequality violation, Phys. Rev. A **108**, 053715 (2023).

[60] A.-L. E. Römling, A. Vivas-Viaña, C. S. Muñoz, and A. Kamra, Resolving nonclassical magnon composition of a magnetic ground state via a qubit, Phys. Rev. Lett. **131**, 143602 (2023).

[61] J. Bylander, S. Gustavsson, F. Yan, F. Yoshihara, K. Harrabi, G. Fitch, D. G. Cory, Y. Nakamura, J.-S. Tsai, and W. D. Oliver, Noise spectroscopy through dynamical decoupling with a superconducting flux qubit, Nat. Phys. **7**, 565 (2011).

[62] S.-L. Ma, J.-K. Xie, and F.-L. Li, Generation of superposition coherent states of microwave fields via dissipation of a superconducting qubit with broken inversion symmetry, Phys. Rev. A **99**, 022302 (2019).

[63] X. Zhu, S. Saito, A. Kemp, K. Kakuyanagi, S.-i. Karimoto, H. Nakano, W. J. Munro, Y. Tokura, M. S. Everitt, K. Nemoto, M. Kasu, N. Mizuochi, and K. Semba, Coherent coupling of a superconducting flux qubit to an electron spin ensemble in diamond, Nature (London) **478**, 221 (2011).

[64] F. Yan, S. Gustavsson, A. Kamal, J. Birenbaum, A. P. Sears, D. Hover, T. J. Gudmundsen, D. Rosenberg, G. Samach, S. Weber, J. L. Yoder, T. P. Orlando, J. Clarke, A. J. Kerman, and W. D. Oliver, The flux qubit revisited to enhance coherence and reproducibility, Nat. Commun. **7**, 12964 (2016).

[65] M. J. Schwarz, J. Goetz, Z. Jiang, T. Niemczyk, F. Deppe, A. Marx, and R. Gross, Gradiometric flux qubits with a tunable gap, New J. Phys. **15**, 045001 (2013).

[66] I. C. Skogvoll, J. Lidal, J. Danon, and A. Kamra, Tunable anisotropic quantum Rabi model via a magnon–spin-qubit ensemble, Phys. Rev. Appl. **16**, 064008 (2021).

[67] T. Holstein and H. Primakoff, Field dependence of the intrinsic domain magnetization of a ferromagnet, Phys. Rev. **58**, 1098 (1940).

[68] C. Kittel, On the theory of ferromagnetic resonance absorption, Phys. Rev. **73**, 155 (1948).

[69] A. Blais, J. Gambetta, A. Wallraff, D. I. Schuster, S. M. Girvin, M. H. Devoret, and R. J. Schoelkopf, Quantum-information processing with circuit quantum electrodynamics, Phys. Rev. A **75**, 032329 (2007).

[70] M. Mirrahimi, Z. Leghtas, V. V. Albert, S. Touzard, R. J. Schoelkopf, L. Jiang, and M. H. Devoret, Dynamically protected cat-qubits: A new paradigm for universal quantum computation, New J. Phys. **16**, 045014 (2014).

[71] Z. Leghtas, S. Touzard, I. M. Pop, A. Kou, B. Vlastakis, A. Petrenko, K. M. Sliwa, A. Narla, S. Shankar, M. J. Hatridge, M. Reagor, L. Frunzio, R. J. Schoelkopf, M. Mirrahimi, and M. H. Devoret, Confining the state of light to a quantum manifold by engineered two-photon loss, Science **347**, 853 (2015).

[72] S. Klingler, H. Maier-Flaig, C. Dubs, O. Surzhenko, R. Gross, H. Huebl, S. T. B. Goennenwein, and M. Weiler, Gilbert damping of magnetostatic modes in a yttrium iron garnet sphere, Appl. Phys. Lett. **110**, 092409 (2017).

[73] D. F. James and J. Jerke, Effective Hamiltonian theory and its applications in quantum information, Can. J. Phys. **85**, 625 (2007).